High-Temperature Electromechanical Characterization of AlN Single Crystals

Taeyang Kim, Jinwook Kim, Rafael Dalmau, Raoul Schlesser, Edward Preble, and Xiaoning Jiang, *Member, IEEE*

***Abstract*—Hexagonal AlN is a non-ferroelectric material and does not have any phase transition up to its melting point (>2000°C), which indicates the potential use of AlN for high-temperature sensing. In this work, the elastic, dielectric, and piezoelectric constants of AlN single crystals were investigated at elevated temperatures up to 1000°C by the resonance method. We used resonators of five different modes to obtain a complete set of material constants of AlN single crystals. The electrical resistivity of AlN at elevated temperature (1000°C) was found to be greater than $5 \times 10^{10}\,\Omega \cdot$ cm. The resonance frequency of the resonators, which was mainly determined by the elastic compliances, decreased linearly with increasing temperature, and was characterized by a relatively low temperature coefficient of frequency, in the range of −20 to −36 ppm/°C. For all the investigated resonator modes, the elastic constants and the electromechanical coupling factors exhibited excellent temperature stability, with small variations over the full temperature range, <11.2% and <17%, respectively. Of particular significance is that due to the pyroelectricity of AlN, both the dielectric and the piezoelectric constants had high thermal resistivity even at extreme high temperature (1000°C). Therefore, high electrical resistivity, temperature independence of electromechanical properties, as well as high thermal resistivity of the elastic, dielectric, and piezoelectric properties, suggest that AlN single crystals are a promising candidate for high-temperature piezoelectric sensing applications.**

I. Introduction

High-temperature (>1000°C) sensors, actuators, and transducers are in great demand for the automotive, aerospace, and energy industries. In aerospace propulsion systems, high-temperature (HT) sensors are required for intelligent propulsion system design, operation, and system maintenance [1]–[3]. These sensors need to be deployed directly inside jet engines because of reliability and noise requirements, and hence, they should be able to withstand a temperature range of 500 to 1000°C for a mission lifetime up to 100 000 h [4]. Additionally, nuclear power industries require a high-temperature sensing technique for various non-destructive testing (NDT) and non-destructive evaluation (NDE) applications [5], [6]. For example, in the typical secondary coolant system of nuclear power plants, ultrasonic NDT of steel components is usually performed at temperatures up to 400°C [7].

Several piezoelectric materials have been extensively researched for high-temperature sensing applications, including quartz (SiO_2), gallium orthophosphate ($GaPO_4$), langasite (LGS), and yttrium calcium oxyborate (YCOB). The most common HT piezoelectric material, quartz, possesses high electrical resistivity (>10^{17} Ω·cm at room temperature), high mechanical quality factor, and excellent high-temperature stability. Nevertheless, its low electromechanical and piezoelectric coefficients, high losses above ~450°C, and α to β phase transition temperature of 573°C limit the use of quartz for applications at temperatures above 600°C [4]–[6]. $GaPO_4$ shows features similar to quartz, such as high electrical resistivity and mechanical quality factor, but it also exhibits high electromechanical coupling and greater piezoelectric sensitivity until the α to β phase transition occurs (<970°C). However, decreased mechanical quality factor due to increased structural disorder at temperatures above 700°C limits its usage [8]–[10]. Langasite crystal, which does not undergo a phase transition before its melting point (1470°C), also has been extensively studied for high-temperature applications. However, the sensing performance of langasite sensors can be limited due to its relatively low electrical resistivity (<10^9 Ω·cm) and low quality factor at elevated temperatures, which result from oxygen ion transport and diffusion in the lattice [11]–[13]. YCOB crystal, which is one of the rare earth calcium oxyborate single crystals $ReCa_4O(BO_3)_3$, has also gained special attention for ultra-high temperature applications. YCOB is known as a promising candidate for HT sensors due to its stable piezoelectric properties and no phase transformation before the melting temperature of 1500°C, as well as exceptional high resistivity [14], [15].

Recently, AlN (wurtzite structure, 6mm crystal class) has gained special attention for ultra-high-temperature applications [16], [17]. The ability to operate in harsh environments makes AlN a promising candidate for SAW and BAW applications such as resonators, filters, and sensors. AlN does not undergo any phase transition up to its melting point (>2000°C), so the piezoelectric response in AlN can be observed up to ultra-high temperatures (>1000°C). Other benefits of AlN include high thermal conductivity (2.85 W/cm·K), high electrical resistivity (10^{11} to 10^{13} Ω·cm), optical transparency in the UV through IR range, and a relatively small thermal expansion coefficient (4.5×10^{-6}/°C) [18].

Manuscript received July 9, 2015; accepted August 15, 2015. The work was supported by the provost doctoral recruitment fellowship (2014–2015) from North Carolina State University.

T. Kim, J. Kim, and X. Jiang are with the Department of Mechanical and Aerospace Engineering, North Carolina State University, Raleigh, NC 27695, USA (e-mail: xjing5@ncsu.edu).

R. Dalmau, R. Schlesser, and E. Preble are with HexaTech Inc., Morrisville, NC 27560, USA.

DOI http://dx.doi.org/10.1109/TUFFC.2015.007252

The elastic and piezoelectric properties of AlN bulk single crystalline and thin film samples have been characterized by various experimental methods at room temperature. Sotnikov *et al.* measured the dielectric, elastic, and piezoelectric constants of AlN single crystals using the ultrasonic pulse-echo and resonance methods [18]. McNeil *et al.* characterized the elastic constants of AlN single crystals with the Brillouin light scattering method [19]. Bu *et al.* obtained the elastic constants of AlN thin films by the SAW technique [20]. Ohashi *et al.* obtained the basic acoustic properties of AlN single crystals through the ultrasonic microspectroscopy technology [21]. However, the properties of AlN single crystals at elevated temperatures (~1000°C) have not been previously reported, in spite of its promising feasibility for high-temperature applications.

Thus in this paper, we report on measurements of the elastic, dielectric, and piezoelectric constants of AlN single crystal at elevated temperatures (up to 1000°C) by using the resonance method.

II. Material Constants Characterization

AlN single crystals (AlN-10 specification) were obtained from HexaTech Inc. (Morrisville, NC, USA), which has successfully combined high-temperature physical vapor transport (PVT) and seeded boule growth for the reproducible production of high structural quality AlN single crystals. The AlN-10 wafer specification consists of single crystal AlN that has no misoriented or poly-crystalline grains, X-ray rocking curve widths typically less than 30 arc-seconds, and typical dislocation densities below $10^4/\text{cm}^2$. Seeded growth enables the fabrication of AlN boules of pre-defined crystallographic orientation that replicate the high quality of the underlying seed. AlN boules were grown along [0 0 0 1] (*c*-direction), and AlN samples were cut from the as-grown boules with the electrode surfaces normal to the *c*-axis except for TS mode sample (parallel to the *c*-axis). Electrode surfaces and sidewalls were then lapped and ground.

The AlN single crystals have 6mm symmetry and thus ten independent material constants in total: five elastic constants (c_{11}^{E}, c_{12}^{E}, c_{13}^{E}, c_{33}^{E}, c_{44}^{E}), three piezoelectric constants (d_{31}, d_{33}, d_{15}), and two dielectric constants ($\varepsilon_{11}^{\mathrm{T}}$, $\varepsilon_{33}^{\mathrm{T}}$) [22], [23]. These constants can be expressed as matrices in (1)–(3).

$$c^{\mathrm{E}} = \begin{bmatrix} c_{11}^{\mathrm{E}} & c_{12}^{\mathrm{E}} & c_{13}^{\mathrm{E}} & 0 & 0 & 0 \\ c_{12}^{\mathrm{E}} & c_{11}^{\mathrm{E}} & c_{13}^{\mathrm{E}} & 0 & 0 & 0 \\ c_{13}^{\mathrm{E}} & c_{13}^{\mathrm{E}} & c_{33}^{\mathrm{E}} & 0 & 0 & 0 \\ 0 & 0 & 0 & c_{44}^{\mathrm{E}} & 0 & 0 \\ 0 & 0 & 0 & 0 & c_{44}^{\mathrm{E}} & 0 \\ 0 & 0 & 0 & 0 & 0 & c_{66}^{\mathrm{E}} \end{bmatrix}, \tag{1}$$

$$d = \begin{bmatrix} 0 & 0 & 0 & 0 & d_{15} & 0 \\ 0 & 0 & 0 & d_{15} & 0 & 0 \\ d_{31} & d_{31} & d_{33} & 0 & 0 & 0 \end{bmatrix}, \tag{2}$$

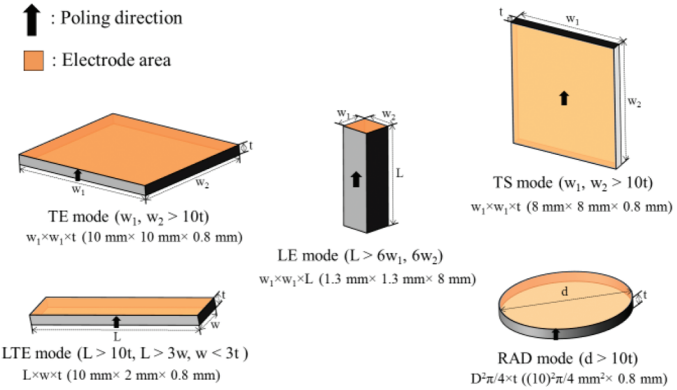

Fig. 1. Geometry of piezoelectric resonators used to identify the material constants.

$$\varepsilon^{\mathrm{T}}/\varepsilon_0 = \begin{bmatrix} \varepsilon_{11}^{\mathrm{T}}/\varepsilon_0 & 0 & 0 \\ 0 & \varepsilon_{11}^{\mathrm{T}}/\varepsilon_0 & 0 \\ 0 & 0 & \varepsilon_{33}^{\mathrm{T}}/\varepsilon_0 \end{bmatrix}, \tag{3}$$

in which the subscripts E and T indicate the condition of constant electrical field and stress, respectively.

Several methods, such as static and quasi-static, resonance, pulse-echo ultrasonic techniques, and their combinations have been used to identify the material constants of piezoelectric materials [18]–[21]. In comparison with other methods, the resonance method is regarded as providing fairly accurate results, and it is considered to be easy to use as long as samples with the required shapes and dimensions are used [21], [24]. Therefore, in this paper, the resonance method was used to determine the properties by analyzing the resonance and antiresonance frequencies of the resonators. The resonance and antiresonance frequencies were obtained from impedance-phase gain analyzer (Agilent 4294A, Agilent Technologies Inc., Santa Clara, CA, USA).

As described in the previous papers and IEEE standards [25], [26], resonators of five different modes were used to obtain a complete set of material constants of AlN single crystals, as shown in Fig. 1: TE (thickness extension), LE (length extension), TS (thickness shear), LTE (length thickness extension), and RAD (radial) resonators. The geometry of each resonator was set to meet the dimensional requirements denoted in Fig. 1 to preserve the resonance of each pure mode.

LTE mode samples with dimensions $L > 10t$, $L > 3w$, $w < 3t$, were used to determine the lateral coupling factor k_{31} and elastic compliances s_{11}^{E}, s_{11}^{D}. The formulae are as follows:

$$k_{31}^2/(k_{31}^2 - 1) = \pi f_{\mathrm{a}}/(2f_{\mathrm{r}}) \cdot \cot\left(\pi f_{\mathrm{a}}/(2f_{\mathrm{r}})\right), \tag{4}$$

$$s_{11}^{\mathrm{E}} = 1/(4\rho(Lf_{\mathrm{r}})^2), \quad s_{11}^{\mathrm{D}} = s_{11}^{\mathrm{E}}(1 - k_{31}^2), \tag{5}$$

where f_{r} is the resonance frequency, f_{a} is the anti-resonance frequency of the lateral mode, ρ is the density of AlN (= 3260 kg/m^3), and the superscripts E and D indicate the conditions of constant electrical field and displacement, respectively.

By using TE mode samples, the electromechanical coupling factor k_t and the elastic constants c_{33}^{D}, c_{33}^{E} were calculated from

$$k_t^2 = \pi f_{\mathrm{r}}/(2f_{\mathrm{a}}) \cdot \cot(\pi f_{\mathrm{r}}/(2f_{\mathrm{a}})), \tag{6}$$

$$c_{33}^{\mathrm{D}} = 4\rho(tf_{\mathrm{a}})^2, \quad c_{33}^{\mathrm{E}} = c_{33}^{\mathrm{D}}(1-k_t^2). \tag{7}$$

Similarly, LE mode samples were used to measure the longitudinal electromechanical coupling factor k_{33} and elastic compliances s_{33}^{D}, s_{33}^{E} using

$$k_{33}^2 = \pi f_{\mathrm{r}}/(2f_{\mathrm{a}}) \cdot \cot(\pi f_{\mathrm{r}}/(2f_{\mathrm{a}})), \tag{8}$$

$$s_{33}^{\mathrm{D}} = 1/(4\rho(Lf_{\mathrm{a}})^2), \quad s_{33}^{\mathrm{E}} = s_{33}^{\mathrm{D}}/(1-k_{33}^2). \tag{9}$$

TS mode samples were used to determine the elastic constants c_{44}^{D}, c_{44}^{E}; elastic compliances s_{44}^{D}, s_{44}^{E}; and coupling factor k_{15} using

$$k_{15}^2 = \pi f_{\mathrm{r}}/(2f_{\mathrm{a}}) \cdot \cot(\pi f_{\mathrm{r}}/(2f_{\mathrm{a}})), \tag{10}$$

$$c_{44}^{\mathrm{D}} = 4\rho(tf_{\mathrm{a}})^2, \quad c_{44}^{\mathrm{E}} = c_{44}^{\mathrm{D}}(1-k_{15}^2), \tag{11}$$

$$s_{44}^{\mathrm{D}} = 1/c_{44}^{\mathrm{D}}, \quad s_{44}^{\mathrm{E}} = 1/c_{44}^{\mathrm{E}}. \tag{12}$$

Lastly, RAD mode samples were used to measure the elastic compliances s_{12}^{E}, s_{12}^{D} based on the planar Poisson's ratio (σ^{P}), following (13). In (13), Poisson's ratio (σ^{P}) can be obtained by calculating the ratio of the resonance frequency of the planar mode ($f_{\mathrm{r}0}$) to the harmonic resonance frequency ($f_{\mathrm{r}1}$), which is previously derived [29].

$$s_{12}^{\mathrm{E}} = -\sigma^{\mathrm{P}} \cdot s_{11}^{\mathrm{E}}, \quad s_{12}^{\mathrm{D}} = s_{12}^{\mathrm{E}} - k_{31}^2 \cdot s_{11}^{\mathrm{E}}. \tag{13}$$

The other elastic compliances s_{13}^{E}, s_{66}^{E} were derived from the above values using the following stiffness-compliance relation for the 6mm crystal group:

$$s_{13}^{\mathrm{E}} = \sqrt{\left[s_{33}^{\mathrm{E}}(s_{11}^{\mathrm{E}}+s_{12}^{\mathrm{E}}) - (s_{11}^{\mathrm{E}}+s_{12}^{\mathrm{E}})/c_{33}^{\mathrm{E}}\right]/2}, \tag{14}$$

$$s_{66}^{\mathrm{E}} = 1/c_{66}^{\mathrm{E}} = 2(s_{11}^{\mathrm{E}} - s_{12}^{\mathrm{E}}). \tag{15}$$

From the above equations, all the elastic compliances were obtained, so elastic stiffness constants such as c_{11}^{E}, c_{12}^{E}, c_{13}^{E}, c_{33}^{E}, c_{44}^{E}, c_{66}^{E} were determined by applying the inverse matrix calculation process.

Dielectric constants, $\varepsilon_{11}^{\mathrm{T}}$, $\varepsilon_{33}^{\mathrm{T}}$ were calculated using the following (16) and (17), where C_i, t_i, A_i are the measured capacitance, thickness, and cross-sectional area of the resonators along the i direction:

$$\varepsilon_{11}^{\mathrm{T}} = C_1 \cdot t_1/A_1, \tag{16}$$

$$\varepsilon_{33}^{\mathrm{T}} = C_3 \cdot t_3/A_3. \tag{17}$$

The derived dielectric permittivities and coupling factors of each mode were adopted to calculate the piezoelectric charge constants d_{33}, d_{31}, d_{15} according to

$$d_{33} = k_{33}\sqrt{s_{33}^{\mathrm{E}} \cdot \varepsilon_{33}^{\mathrm{T}}}, \tag{18}$$

$$d_{31} = -k_{31}\sqrt{s_{11}^{\mathrm{E}} \cdot \varepsilon_{33}^{\mathrm{T}}}, \tag{19}$$

$$d_{15} = -k_{15}\sqrt{s_{44}^{\mathrm{E}} \cdot \varepsilon_{11}^{\mathrm{T}}}. \tag{20}$$

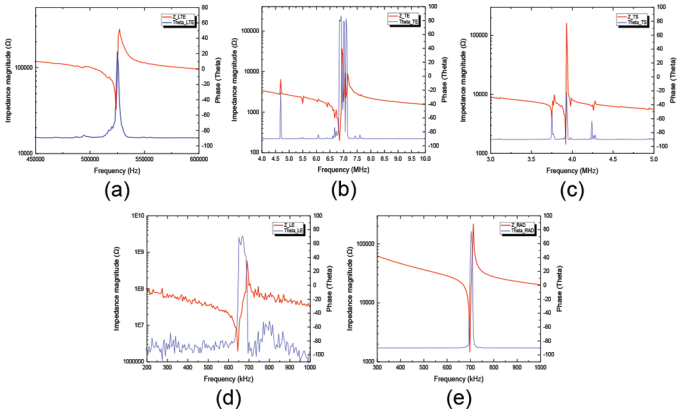

Fig. 2. Impedance spectra of all the samples: (a) LTE, (b) TE, (c) TS, (d) LE, and (e) RAD mode.

In this study, the samples (3 samples each for TE, RAD, TS modes and 4 samples for LTE, LE modes) were dc sputtered with platinum thin films (300 nm thick) on the required parallel surfaces as the electrodes. Platinum was selected as the electrode material because of its high melting temperature (~1768°C). A specially designed sample holder was used for high-temperature measurements. In the sample holder, high-temperature resistive wire (Kanthal A1, Sandvik Inc., Hallstahammar, Sweden), insulator (alumina plate), and housing (Inconel 601, High Performance Alloys Inc., Windfall, IN, USA) were assembled for resistance to high temperature oxidation and corrosion. A vertical tube furnace (model GSL 1100X, MTI Corporation, Richmond, CA, USA) was used to control the temperature. The samples were located at the center of the vertical tube furnace. The furnace was heated up to 1000°C by 100°C increments starting from room temperature with 10 min duration of temperature increment. The furnace was heated to a value (20°C) above the target temperature because the furnace would cool during testing, and then unplugged to reduce the ac electric noise created by the heating units. The signal from the AlN single crystals was obtained from an impedance-phase gain analyzer (Agilent 4294A, Agilent Technologies Inc.). The data were transferred to a computer in Excel (Microsoft Corp., Redmond, WA, USA) format for signal processing and analysis.

III. Results and Discussion

To confirm the reliability of the sample holder, impedance spectra and the capacitances of all samples were measured at room temperature using the impedance-phase gain analyzer (Fig. 2). All of the constants of AlN were then derived according to the above (4)–(20). The comparison between the currently derived constants and published ones [18]–[21], [28] is summarized in Table I. It can be observed that all constants are within 15% of the range of the published data, which indicates the reliability of the specially designed sample holder.

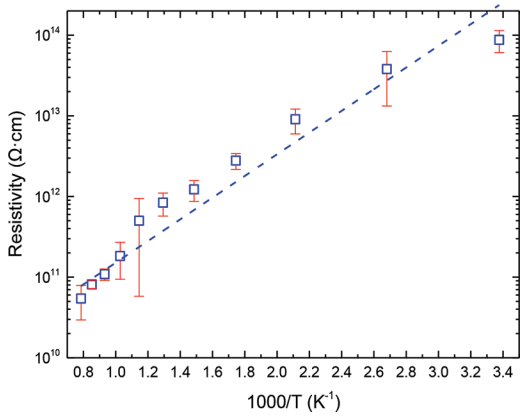

Fig. 3. Electrical resistivity of AlN single crystal as a function of temperature (error bars were amplified by 10 times).

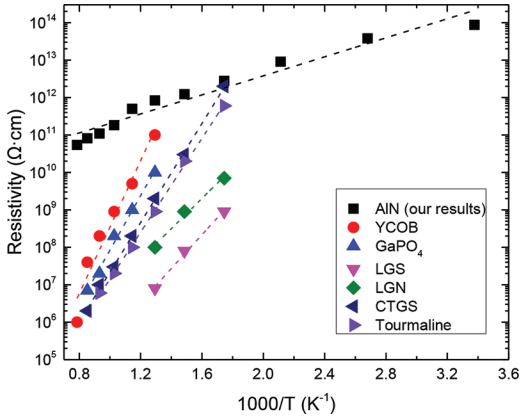

Fig. 4. Electrical resistivity of nonferroelectric, piezoelectric single crystals as a function of temperature.

Electrical resistivity was measured using a Keithley model 6571A electrometer (Keithley Instruments, Cleveland, OH, USA) when applying 100 V across the TE resonators. The resistivity as a function of temperature is given in Fig. 3, in which the dashed line is a linearly fitted line of measured data and error bars were amplified by 10 times for clarification. As shown, AlN single crystals exhibited very high resistivity at room temperature, 8.8×10^{13} Ω·cm, and even at elevated temperature, with values of 1.1×10^{11} Ω·cm and 5.4×10^{10} Ω·cm at 800°C and 1000°C, respectively. The activation energy (E_a) calculated according to Arrhenius law was found to be on the order of 0.28 ± 0.02 eV. Fig. 4 shows the electrical resistivity as a function of temperature for non-ferroelectric, piezoelectric single crystals, where it is observed that LGS crystals possess relatively low resistivity, with the lowest value of 8×10^6 Ω·cm at 500°C. The $GaPO_4$ and YCOB crystals possess relatively high resistivity, on the order of 10^{10} and 10^{11} Ω·cm at 500°C, respectively [3], [9], [13], [29]–[31]. At 900°C, the resistivity of AlN (8×10^{10} Ω·cm) is three orders of magnitude higher than YCOB (4×10^7 Ω·cm), which indicates a high insulation property of AlN required to maintain the developed charge for a long time to be detected by the electronic system.

The thermal frequency stability of AlN was investigated by analyzing the variation of resonance frequencies of all the resonator modes at elevated temperatures. Fig. 5 presents the variation of resonance frequencies of different resonator modes as a function of temperature. It was observed that the resonance frequencies of all the investigated samples were shifted downward linearly with increasing temperature due to the thermal softening effect, where all the resonator modes were found to possess relatively low temperature coefficients of frequency (TCF), in the range of −20 to −36 ppm/°C, comparable with those of YCOB used as high-temperature sensors (with TCF in the range of −45 to −95 ppm/°C [3], [32]).

With the measured resonance and anti-resonance frequencies for all the resonators modes, shown in Fig. 1, at temperatures up to 1000°C, the temperature dependence of elastic compliances was investigated and results are shown in Fig. 6. It was observed that all the elastic compliances increased with increasing temperature, with variations of 4.2 to 7.3%, except for s_{13}^E, with a variation of 11.2% over the full temperature range. s_{13}^E was determined at the last step for elastic compliance calculations. Due to the derivation procedure for elastic compliance constants, s_{13}^E may contain accumulated error. Compared with the values of YCOB single crystals (8.6–19.0% [32]), AlN shows a lower temperature dependence of elastic properties.

The elastic stiffness constants were obtained by calculating the inverse matrix of the determined elastic compliances (Fig. 7). All the elastic stiffness values decreased

TABLE I. MATERIAL CONSTANTS OF AlN (SINGLE CRYSTALS) AT ROOM TEMPERATURE.

Material constant	Single crystal [18]	Single crystal [19]	Single crystal [21]	Single crystal [20], [28]	Single crystal (our results)
c_{11}^E (GPa)	402.5 ± 0.5	410.5 ± 10	401.2 ± 0.5	—	412.6 ± 0.5
c_{12}^E (GPa)	135.6 ± 0.5	148.5 ± 10	135 ± 0.5	—	126.6 ± 0.5
c_{13}^E (GPa)	101 ± 2.0	98.9 ± 3.5	96.3 ± 22.1	—	118.8 ± 0.9
c_{33}^E (GPa)	387.6 ± 1.0	388.5 ± 10	368.2 ± 27.9	—	386.1 ± 4.5
c_{44}^E (GPa)	122.9 ± 0.5	124.6 ± 4.5	122.6 ± 0.2	122 ± 1	127.4 ± 0.9
e_{31} (C/m^2)	−0.6 ± 0.2	—	−0.12 ± 1.09	−0.58 ± 0.23	−0.47 ± 0.2
e_{33} (C/m^2)	1.34 ± 0.1	—	1.84 ± 0.71	1.39 ± 0.22	2.09 ± 0.4
e_{15} (C/m^2)	−0.32 ± 0.05	—	−0.26 ± 0.03	−0.29 ± 0.06	−0.24 ± 0.05
$\varepsilon_{11}/\varepsilon_0$	9 ± 0.1	—	—	8.5	8.44 ± 0.1
$\varepsilon_{33}/\varepsilon_0$	9.5 ± 0.1	—	—	8.5	10.51 ± 0.1

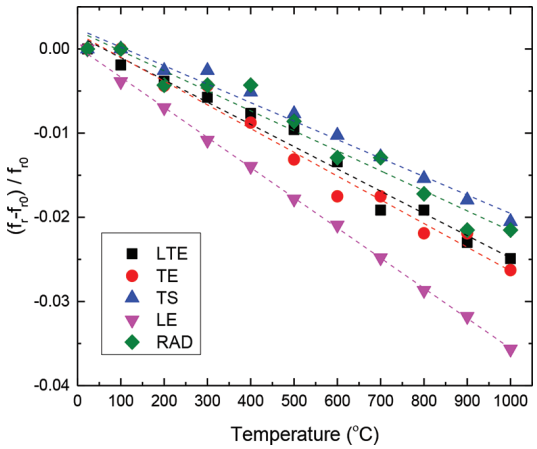

Fig. 5. Temperature dependence of resonance frequency for all the samples.

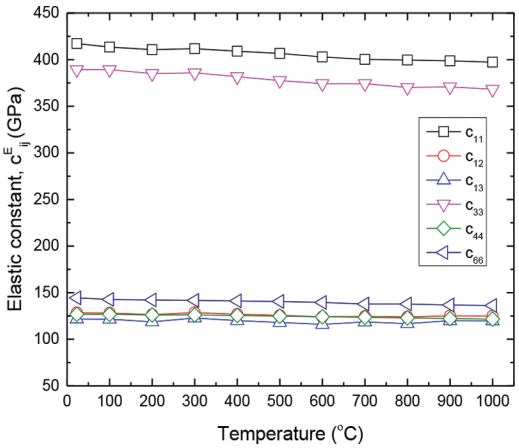

Fig. 7. Variation of elastic stiffness constants as a function of temperature.

with increasing temperature, with variation of −1.7 to −5.6%.

The electromechanical coupling factors k_{ij} indicate the effectiveness with which a piezoelectric material converts electrical energy into mechanical energy or vice versa. After measuring the resonance and anti-resonance frequencies at elevated temperatures, the variation of k_{ij} as a function of temperature was obtained (Fig. 8). It can be noted that the LE mode resonator showed the highest electromechanical coupling factor, with k_{33} values of 0.391 and 0.395 at room temperature and 1000°C, respectively, representing a variation less than 1.6% over the full temperature range. In addition, the TE and LTE mode resonators exhibited relatively high coupling factors, k_t = 0.178 and k_{31} = 0.119 at room temperature, with values of 0.206 and 0.098 at 1000°C, respectively, giving variations ∼±17%. The coupling factors were found to largely maintain their values up to 1000°C, exhibiting a stable piezoelectricity at elevated temperature.

Dielectric constants K_{11}^{T} and K_{33}^{T}, were derived from capacitance measurements at 1 kHz by using (16) and (17), respectively. Dielectric loss, tan δ, as a function of temperature was measured at 1 kHz, and the results are shown in Fig. 9. All dielectric values increase sharply after 800°C, which can be understood from the strong pyroelectric properties of AlN [33]. As for the increase of dielectric loss at elevated temperature (14.6% at 1000°C), it was reported that AlN surface oxidation, which results in electron energy loss and dissipation [34], starts to occur in the temperature range 800 to 900°C [35], [36]. Nevertheless, results exhibit overall stable dielectric behavior.

After the determination of elastic compliances, electromechanical coupling factors, and dielectric constants, the piezoelectric coefficients were obtained. Fig. 10 shows the variation of piezoelectric coefficients as a function of temperature. The highest piezoelectric coefficient was found from samples in the length extensional mode, with a piezoelectric coefficient d_{33} of 6.5 pC/N at room temperature, increasing to 13.5 pC/N at 1000°C. The lateral and the thickness shear mode piezoelectric coefficients d_{31} and d_{15} show better temperature stability compared with the thickness mode piezoelectric coefficient. Both of the d_{31} and d_{15} values were determined as −1.9 pC/N at room temperature and −3.2 and −3.1 pC/N at 1000°C,

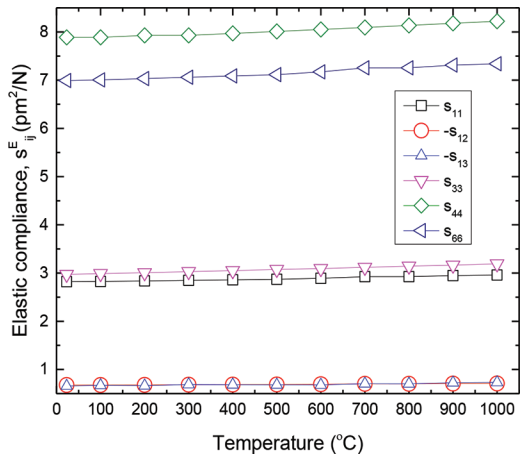

Fig. 6. Variation of elastic compliances as a function of temperature.

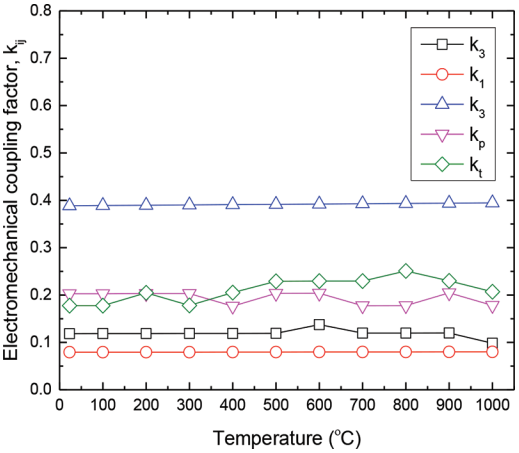

Fig. 8. Variation of electromechanical coupling factors as a function of temperature.

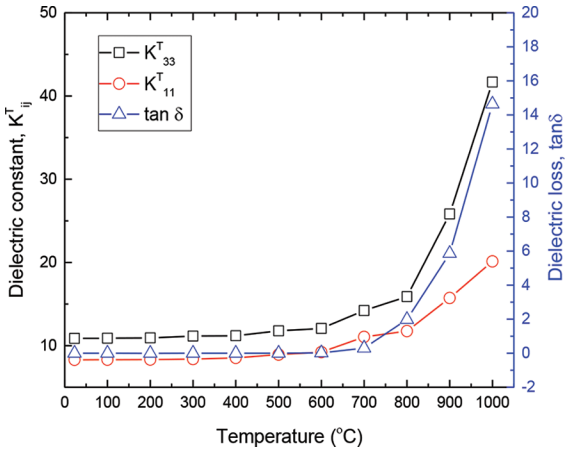

Fig. 9. Dielectric constants and dielectric loss as a function of temperature measured at 1 kHz.

respectively, giving a variation of <60% over the full temperature range. The increase of piezoelectric coefficients at high temperature (800–1000°C) is due to the increased dielectric permittivity, shown in Fig. 9. The thermal resistivity of piezoelectric coefficients of AlN was comparable with the values of YCOB (10–70%) [32].

IV. Conclusions

The electrical resistivity, temperature dependence of the resonance frequency, elastic compliances, electromechanical coupling factors, dielectric constants, dielectric loss, and piezoelectric coefficients of AlN single crystals grown by PVT were investigated in the temperature range of 23°C to 1000°C.

The electrical resistivity of AlN at elevated temperature (1000°C) was found to be greater than 5×10^{10} Ω·cm. The resonance frequency of resonators exhibited a linear decrease with increasing temperature due to the thermal softening effect. This variation showed TCF values in the range of −20 to −36 ppm/°C, comparable with YCOB, which is already used for temperature sensors. For all investigated resonator modes, the elastic constants and the electromechanical coupling factors exhibited excellent temperature stability in comparison with previously reported piezoelectric ceramics and single crystals. Of particular significance is that both the dielectric and the piezoelectric constants had high thermal resistivity even at extreme high temperature due to the pyroelectric properties of AlN. The relative temperature independence of electromechanical properties, as well as the high thermal resistivity of the elastic, dielectric, and piezoelectric properties, suggest that AlN single crystals are a promising candidate for high-temperature piezoelectric sensing applications.

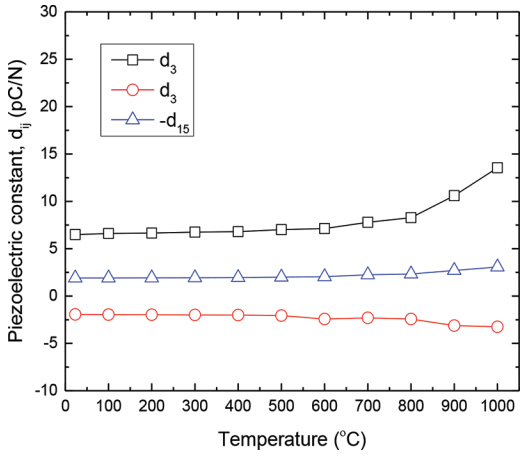

Fig. 10. Variation of piezoelectric coefficients as a function of temperature.

References

[1] G. W. Hunter, J. D. Wrbanek, R. S. Okojie, P. G. Neudeck, G. C. Fralick, L. Chen, J. Xu, G. M. Beheim, N. Glenn, B. Road, and C. P. Road, "Development and application of high temperature sensors and electronics for propulsion applications," *Library (Lond.)*, vol. 6222, pp. 1–12, 2006.

[2] A. P. Carlucci, F. F. Chiara, and D. Laforgia, "Analysis of the relation between injection parameter variation and block vibration of an internal combustion diesel engine," *J. Sound Vibrat.*, vol. 295, no. 1–2, pp. 141–164, 2006.

[3] S. Zhang, Y. Fei, B. H. T. Chai, E. Frantz, D. W. Snyder, X. Jiang, and T. R. Shrout, "Characterization of piezoelectric single crystal Y Ca_4 $O(BO_3)_3$ for high temperature applications," *Appl. Phys. Lett.*, vol. 92, no. 20, art. no. 202905, 2008.

[4] R. C. Turner, P. A. Fuierer, R. E. Newnham, and T. R. Shrout, "Materials for high temperature acoustic and vibration sensors: A review," *Appl. Acoust.*, vol. 41, no. 4, pp. 299–324, 1994.

[5] H. Lee and H. Sohn, "Damage detection technique by measuring laser-based mechanical impedance," *Rev. Prog. Quant. NDE*, vol. 1581, no. 1, pp. 429–436, 2014.

[6] J. H. Park, J. H. Lee, G. C. Seo, and S. W. Choi, "Application of laser-generated ultrasound for evaluation of thickness reduction in carbon steel pipes," *Key Eng. Mater.*, vol. 321–323, pp. 743–746, Oct. 2006.

[7] R. Kažys, A. Voleišis, and B. Voleišienė, "High temperature ultrasonic transducers: Review," *Ultrasound*, vol. 63, no. 2, pp. 7–17, 2008.

[8] M. Schulz, J. Sauerwald, D. Richter, and H. Fritze, "Electromechanical properties and defect chemistry of high-temperature piezoelectric materials," *Ionics (Kiel)*, vol. 15, no. 2, pp. 157–161, 2009.

[9] S. Zhang and F. Yu, "Piezoelectric materials for high temperature sensors," *J. Am. Ceram. Soc.*, vol. 94, no. 10, pp. 3153–3170, 2011.

[10] D. Damjanovic and D. Darnjanovic, "Materials for high temperature piezoelectric transducers," *Curr. Opin. Solid State Mater. Sci.*, vol. 3, no. 5, pp. 469–473, 1998.

[11] H. Fritze, H. Seh, H. L. Tuller, and G. Borchardt, "Operation limits of langasite high temperature nanobalances," *J. Eur. Ceram. Soc.*, vol. 21, no. 10–11, pp. 1473–1477, 2001.

[12] H. Fritze, "High-temperature bulk acoustic wave sensors," *Meas. Sci. Technol.*, vol. 22, no. 1, art. no. 012002, 2010.

[13] S. Zhang, Y. Zheng, H. Kong, J. Xin, E. Frantz, and T. R. Shrout, "Characterization of high temperature piezoelectric crystals with an ordered langasite structure," *J. Appl. Phys.*, vol. 105, no. 11, pp. 1–6, 2009.

[14] K. Kim, S. Zhang, G. Salazar, and X. Jiang, "Design, fabrication and characterization of high temperature piezoelectric vibration sensor using YCOB crystals," *Sens. Actuators A Phys.*, vol. 178, pp. 40–48, May 2012.

[15] X. Jiang, K. Kim, S. Zhang, J. Johnson, and G. Salazar, "High-temperature piezoelectric sensing," *Sensors (Basel)*, vol. 14, no. 1, pp. 144–169, 2013.

[16] E. Ruiz, S. Alvarez, and P. Alemany, "Electronic structure and properties of AlN," *Phys. Rev. B Condens. Matter*, vol. 49, no. 11, pp. 7115–7123, 1994.
[17] D. A. Parks, B. R. Tittmann, and M. M. Kropf, "Aluminum nitride as a high temperature transducer," in *AIP Conf. Proc.*, 2010, vol. 1211, pp. 1029–1034.
[18] A. Sotnikov, H. Schmidt, M. Weihnacht, E. Smirnova, T. Chemekova, and Y. Makarov, "Elastic and piezoelectric properties of AlN and $LiAlO_2$ single crystals," *IEEE Trans. Ultrason. Ferroelectr. Freq. Control*, vol. 57, no. 4, pp. 808–811, 2010.
[19] L. E. McNeil, M. Grimsditch, and R. H. French, "Vibrational spectroscopy of aluminum nitride," *J. Am. Ceram. Soc.*, vol. 76, no. 5, pp. 1132–1136, 1993.
[20] G. Bu, D. Ciplys, M. Shur, L. J. Schowalter, S. Schujman, and R. Gaska, "Surface acoustic wave velocity in single-crystal AIN substrates," *IEEE Trans. Ultrason. Ferroelectr. Freq. Control*, vol. 53, no. 1, pp. 251–254, 2006.
[21] Y. Ohashi, M. Arakawa, J. I. Kushibiki, B. M. Epelbaum, and A. Winnacker, "Ultrasonic microspectroscopy characterization of AlN single crystals," *Appl. Phys. Express*, vol. 1, no. 7, art. no. 0770041, 2008.
[22] R. E. Newnham, *Properties of Materials Anisotropy, Symmetry, Structure Anisotropy*. New York, NY, USA: Oxford, 2005.
[23] K. Tsubouchi, K. Sugai, and N. Mikoshiba, "AlN material constants evaluation and SAW properties on AlN/Al_2O_3 and AlN/Si," in *IEEE Ultrason. Symp.*, 1981, pp. 375–380.
[24] C. Joh, J. Kim, and Y. Roh, "Determination of the complex material constants of PMN–28%PT piezoelectric single crystals," *Smart Mater. Struct.*, vol. 22, no. 12, art. no. 125027, 2013.
[25] S. H. Lee and Y. Roh, "Characterization of all the elastic, piezoelectric, and dielectric constants of tetragonal $Pb(Mg_{1/3}Nb_{2/3})O_3$–$PbTiO_3$ single crystals," *Jpn. J. Appl. Phys.*, vol. 46, no. 7B, pp. 4462–4465, 2007.
[26] IEEE Standard on Piezoelectricity. ANSI/IEEE Std., 176, 1987.
[27] A. H. Meitzler, H. M. J. O'Bryan, and H. F. Tiersten, "Definition and measurement of radial mode coupling factors in piezoelectric ceramic materials with large variations in Poisson's ratio," *IEEE Trans. Sonics Ultrason.*, vol. 20, no. 3, pp. 233–239, 1973.
[28] G. Bu, D. Ciplys, M. Shur, L. J. Schowalter, S. Schujman, and R. Gaska, "Electromechanical coupling coefficient for surface acoustic waves in single-crystal bulk aluminum nitride," *Appl. Phys. Lett.*, vol. 84, no. 23, pp. 4611–4613, 2004.
[29] S. Zhang, A. Yoshikawa, K. Kamada, E. Frantz, R. Xia, D. W. Snyder, T. Fukuda, and T. R. Shrout, "Growth and characterization of high temperature LNGA and LTGA piezoelectric single crystals," *Solid State Commun.*, vol. 148, no. 5–6, pp. 213–216, 2008.
[30] S. Zhang, T. R. Shrout, Y. T. Fei, B. H. T. Chai, E. Frantz, and D. W. Snyder, "High temperature piezoelectric single crystal $ReCa_4O(BO_3)_3$ for sensor application," *IEEE Trans. Ultrason. Ferroelectr. Freq. Control*, vol. 55, no. 12, pp. 2703–2708, 2008.
[31] S. Zhang, F. P. Yu, R. Xia, Y. T. Fei, E. Frantz, X. Zhao, D. R. Yuan, B. H. T. Chai, D. Snyder, and T. R. Shrout, "High temperature ReCOB-piezocrystals: Recent developments," *J. Cryst. Growth*, vol. 318, no. 1, pp. 884–889, 2011.
[32] F. Yu, X. Duan, S. Zhang, Y. Yu, T. Ma, and X. Zhao, "Temperature dependence of electro-elastic properties of yttrium calcium oxyborate single crystals," in *2012 Symp. on Piezoelectricity, Acoustic Waves and Device Applications*, pp. 293–297.
[33] W. S. Yan, R. Zhang, X. Q. Xiu, Z. L. Xie, P. Han, R. L. Jiang, S. L. Gu, Y. Shi, and Y. D. Zheng, "Temperature dependence of the pyroelectric coefficient and the spontaneous polarization of AlN," *Appl. Phys. Lett.*, vol. 90, no. 21, art. no. 212102, 2007.
[34] M. Sternitzke, "Growth of oxide layers on thin aluminum nitride samples measured by electron energy-loss spectroscopy," *J. Am. Ceram. Soc.*, vol. 76, no. 195, pp. 2289–2294, 1993.
[35] J. W. Lee, I. Radu, and M. Alexe, "Oxidation behavior of AlN substrate at low temperature," *J. Mater. Sci. Mater. Electron.*, vol. 13, no. 3, pp. 131–137, 2002.
[36] R. Kazys, A. Voleisis, R. Sliteris, L. Mazeika, R. Van Nieuwenhove, P. Kupschus, and H. A. Abderrahim, "High temperature ultrasonic transducers for imaging and measurements in a liquid Pb/Bi eutectic alloy," *IEEE Trans. Ultrason. Ferroelectr. Freq. Control*, vol. 52, no. 4, pp. 525–537, 2005.

Taeyang Kim received his B.S. degree in mechanical engineering from the Korea Military Academy, Seoul, Korea, in 2005, and his M.S. degree in mechanical engineering from Texas A&M University, College Station, Texas, in 2009. In 2014, he joined Dr. Xiaoning Jiang's Micro/Nano Engineering Lab at North Carolina State University, working on smart materials, structures, and applications. He is also interested in design and fabrication of piezoelectric sensors that are used for shear stress measurement.

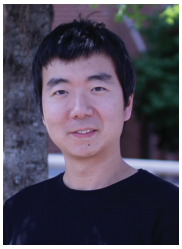

Jinwook Kim received his B.S. and M.S. degrees in mechanical engineering from Kyungpook National University in 2010 and 2012, respectively, working on design and optimization of underwater transducers. In 2013, he joined Dr. Xiaoning Jiang's Micro/Nano Engineering Lab at North Carolina State University, working on the design and fabrication of ultrasound transducers for diagnosis and noninvasive therapy. His broad research interests involve laser-generated ultrasound, ultrasound-mediated therapies, and bio-sensors.

Rafael Dalmau received the B.S. degree in physics from the University of Puerto Rico, Río Piedras, PR, in 1999 and the Ph.D. degree in materials science and engineering from North Carolina State University (NCSU), Raleigh, North Carolina, in 2005.

From 2001 to 2005 he was a Research Assistant and GAANN Fellow in the Wide Bandgaps Laboratory at NCSU, where he developed vapor growth of AlN single crystals, and from 2005 to 2007 he was a Post-Doctoral Research Assistant at NCSU, studying MOVPE growth of nitrides. Since 2007, he has been a Senior Process Engineer at HexaTech Inc., Morrisville, North Carolina, where he heads the wafer processing department. He is the author and co-author of two book chapters, four issued US patents, and over 45 peer-reviewed journal publications. His research interests include growth and processing of wide-bandgap nitride crystals, nitride optoelectronic devices, and high-power electronics.

Raoul Schlesser received a Ph.D. degree in physics from the Swiss Federal Institute of Technology (ETH) in Zürich, Switzerland in 1996. From 1996 until 2005, he held various positions at the Department of Materials Science and Engineering at North Carolina State University (NCSU), and where, as a Research Associate Professor, he focused on the development of III-nitride growth techniques and, particularly, the growth of AlN bulk single crystals.

At present, he is the Vice President of Crystal and Wafer Development at HexaTech Inc., a startup company that he co-founded and that specializes in the fabrication of highest-quality AlN single crystals, as well as related wafer products and III-nitride devices.

Edward A. Preble received the B.S. degree in mechanical engineering from Worcester Polytechnic Institute in Worcester, Massachusetts, in 1993, and received both the M.S. degree in nuclear engineering in 1996 and the Ph.D. degree in materials science and engineering in 2001 from North Carolina State University (NCSU) in Raleigh.

From 2001 to 2003, he was a postdoctoral researcher at NCSU focused on the growth of SiC by MOCVD and the characterization of GaN thin-film epitaxy. From 2003 to 2013, he held several engineering positions, as well as the COO, CTO, and CMO positions at Kyma Technologies, a company focused on the commercialization of bulk GaN sub-

strates grown by HVPE and AlN grown by PVD. Since 2014, he has been a senior process engineer at HexaTech, where he manages the production of bulk AlN crystals grown by PVT. Dr. Preble has co-authored over 75 peer-reviewed publications and has seven issued US patents.

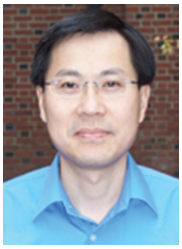

Xiaoning Jiang received his B.S. degree in mechanical engineering from Shanghai Jiaotong University in 1990, his M.S. degree in mechanical engineering from Tianjin University in 1992, and his Ph.D. degree in precision instruments from Tsinghua University in 1997. He received postdoctoral training from Nanyang Technological University and Pennsylvania State University from 1997 to 2001. He joined Standard MEMS Inc. as an R&D Engineer in 2001 and then worked for TRS Technologies Inc. as a Research Scientist, Senior Scientist, Chief Scientist, and Vice President for Technology before joining North Carolina State University in 2009. He is now a Professor of Mechanical and Aerospace Engineering and an Adjunct Professor of Biomedical Engineering. Dr. Jiang is the author and co-author of two book chapters, one book, nine issued US patents, and more than ten US patent applications, more than 63 peer-reviewed journal papers, and more than 65 conference papers on piezoelectric composite micromachined ultrasound transducers, ultrasound for medical imaging and therapy, NDE, smart materials and structures, and M/NEMS. Dr. Jiang is a member of the technical program committee for IEEE UFFC. He is also a Guest Editor for the journal *Sensors*.